Engineering Science and Technology, an International Journal 19 (2016) 1864–1870

HOSTED BY

Contents lists available at ScienceDirect

Engineering Science and Technology, an International Journal

journal homepage: www.elsevier.com/locate/jestch

Full Length Article

# Design and analysis of high sensitivity photosensor using Cylindrical Surrounding Gate MOSFET for low power applications

Aakash Jain, Sanjeev Kumar Sharma *, Balwinder Raj

*VLSI Design Lab, Department of ECE, NIT Jalandhar, Punjab 144011, India*

ARTICLE INFO

*Article history:*
Received 19 May 2016
Revised 17 August 2016
Accepted 18 August 2016
Available online 3 September 2016

*Keywords:*
ATLAS-3D
Dark current
CSG MOSFET
Photosensor
Quantum efficiency
Responsivity

ABSTRACT

In this paper, a high sensitivity photosensor is proposed that utilizes the Zinc Oxide (metallic ZnO) which act as a transparent optical window over channel. High sensitivity is achieved by using Cylindrical Surrounding Gate Metal Oxide Semiconductor Field Effect Transistor (CSG MOSFET). On being exposed to light there is substantial increase in conductance and thereby change in the subthreshold current under exposure is utilized as a sensitivity parameter. Most of the Conventional FET based photosensors that are available utilizes threshold voltage as the parameter for sensitivity comparison but in this proposed sensor, under illumination change in the conductance resulting in variation of the subthreshold current is considered to be the sensitivity parameter. Performance comparison with Double Gate Metal Oxide Semiconductor Field Effect Transistor (DG MOSFET) in terms of sensitivity, threshold voltage and $I_{on}/I_{off}$ ratio is also done and observed results shows that CSG MOSFET is an ideal candidate for being used as a high sensitivity photosensor because in CSG MOSFET due to effective control of gate over channel low dark current, high sensitivity, low threshold voltage and high $I_{on}/I_{off}$ ratio can be achieved. Further impact of channel radius on responsivity ($R_e$), quantum efficiency ($Q_e$) and $I_{on}/I_{off}$ ratio is also studied for the proposed device.



## 1. Introduction

Nowadays the demand of low power and highly sensitive photosensors is growing at an astonishing rate for being used in many application such as in flame detectors, chemical composition analysis, missile plume prediction, medical diagnosis and treatment, surveillance cameras etc. [1–6], and also in optical interconnects for inter chip data communication [7] and in optical storage media [8]. Compatibility of Field Effect Transistors (FETs) for integrated circuit have helped in the successful development of these devices for their use as photosensors. Silicon (Si) based photodetectors are generally being utilized as a part of a large number of these applications because of the fact that they occupy less volume, have high signal to noise ratio, abundantly available and being congenial with microelectronics they are extensively used in the areas of defence and civil applications [9].

Sensitivity is one of the most important parameter which judges the effectiveness of the photosensor. Today most of the research work is totally centered on in using highly photosensitive channel material [10], transparent gate material [11] and back illumination method [12,13] to enhance the photoresponse, but in this paper device engineering is utilized to achieve the targets, as in order to achieve a very low dark current device engineering plays a crucial role. In order to further increase the sensitivity for the desired region of spectrum ZnO as a gate material is utilized which act as an optical filter. ZnO being a transparent gate material for UV–visible spectrum [14] has the benefit of providing less reflection for the desired region of spectrum so that a large portion of light occurrence on the gate material reaches to the semiconductor.

Photodiodes other than MOSFET based i.e. Avalanche photodiodes; PIN photodiode, p-n junction photodiodes etc. have their own limitations. Low $Q_e$ of p-n junction photodiode [15], high noise in avalanche photodiodes [16] and speed limitation due to transit time of the generated photocarriers in PIN photodiode [17] restrict their use as a high sensitivity photosensors and hence MOSFET based photosensor can be effectively used to overcome all these limitations. MOSFET based photosensors dissipate very low power because of very high input impedance, they also introduce less noise due to participation of majority charge carriers and can also withstand high temperature.

As compared to DG MOSFET, CSG MOSFET have several advantages including better electrostatic coupling between gate and the channel as gate electrode completely surrounds the channel and hence off state leakage current gradually decreases, higher $I_{on}/I_{off}$

* Corresponding author.
*E-mail address:* sanjeev.nitj14@gmail.com (S.K. Sharma).
Peer review under responsibility of Karabuk University.

http://dx.doi.org/10.1016/j.jestch.2016.08.013
2215-0986/

ratio for fixed drain voltage and reduced short channel effects (SCEs) [18].

In this paper CSG MOSFET with ZnO as a gate and silicon dioxide ($SiO_2$) as gate dielectric is used for designing high sensitivity low power photosensor. The combined advantageous effect of device engineering and channel material engineering is utilized to achieve our goal of designing a photosensor that can effectively use in UV–visible spectrum applications. In this paper performance comparison with DG MOSFET in terms of dark current, threshold voltage and $I_{on}/I_{off}$ ratio is also done and results shows that CSG MOSFET is superior in performance as a highly sensitive photosensor. Impact of channel radius on responsivity (R), quantum efficiency ($Q_e$) and $I_{on}/I_{off}$ ratio is also studied for the proposed device.

## 2. Device structure and simulation setup

Fig. 1(a) depicts the 2D-cross section view of CSG MOSFET and Fig. 1(b) 3D-Simulated structure of DG MOSFET under incident radiation Fig. 1(c) depicts the 3D-simulated structure of CSG MOSFET under incident radiation. R is the radius of channel, L is the channel length, $L_S$ is the source length, $L_D$ is the drain length, z is the channel direction, and $t_{ox}$ is the oxide thickness.

In order to extricate device characteristics under dark SILVACO ATLAS-3D simulator [19] is utilized to simulate CSG MOSFET. The parameters utilized in simulation process are as given in Table 1. It also incorporates advance LUMINOUS-3D optical device simulator to extricate device characteristics under incident radiation which uses Ray Trace method for calculating the photogeneration rate at defined mesh points. The optical parameters for the incident radiation such as radiation intensity, wavelength and location is set by using BEAM keyword incorporated in LUMINOUS-3D module. Various models used for the purpose of simulation of CSG MOSFET are: Field Dependent Mobility model (FDM) and Shockley Read Hall model (SRH). FDM model takes into consideration the dependence of carrier mobility with high electric field and SRH model accounts for the chances of recombination phenomenon at traps. The thickness of both ZnO as a transparent gate material and $SiO_2$ as a gate dielectric is kept small so that most of the light falling on the gate region reaches Silicon (Si) channel underneath. The path of light from air to the Si channel underneath is obstructed due to reflections at three interfaces namely air to gate (ZnO), gate to oxide ($SiO_2$) and oxide to semiconductor (Si). Reflection at theses interfaces helps in analyzing the behavior of device under incident radiation. The reflection coefficients for these three interfaces can be calculated using the formula [20]:

**Table 1**
Parameters utilized in simulation process.

| Symbol | Definition | Value |
|---|---|---|
| L | Channel length | 1.0 μm |
| $t_{si}$ | Silicon film thickness | 0.5 μm |
| R | Channel radius ($t_{si}$ = 2R) | 0.25 μm |
| $L_S$ | Source length | 0.5 μm |
| $L_D$ | Drain length | 0.5 μm |
| $t_{ox}$ | Oxide thickness | 10 nm |
| $N_A$ | Channel doping | $1 \times 1016\ cm^{-3}$ |
| $N_D$ | Source/Drain doping | $1 \times 1020\ cm^{-3}$ |

$$R_c = \frac{(n_c - n_{c+1})^2 + k_{c+1}^2}{(n_c + n_{c+1})^2 + k_{c+1}^2} \quad (1)$$

where $R_1$, $R_2$ and $R_3$ are the reflection coefficients at the three interfaces i.e. air to gate (ZnO), gate to oxide ($SiO_2$) and oxide to semiconductor (Si) respectively. $n_1$, $n_2$, $n_3$ and $n_4$ are the real part of refractive index of air, gate, oxide and semiconductor respectively and $k_c$'s are the corresponding imaginary part of the refractive indexes. SOPRA database [21] is referred to get the real and imaginary values of the refractive index in order to calculate the reflection coefficients and for the purpose of simulation of CSG MOSFET under incident radiation. Table 2 shows the real and imaginary refractive index values for ZnO, $SiO_2$ and Si for different wavelengths of incident radiation and the calculated reflection coefficients for above

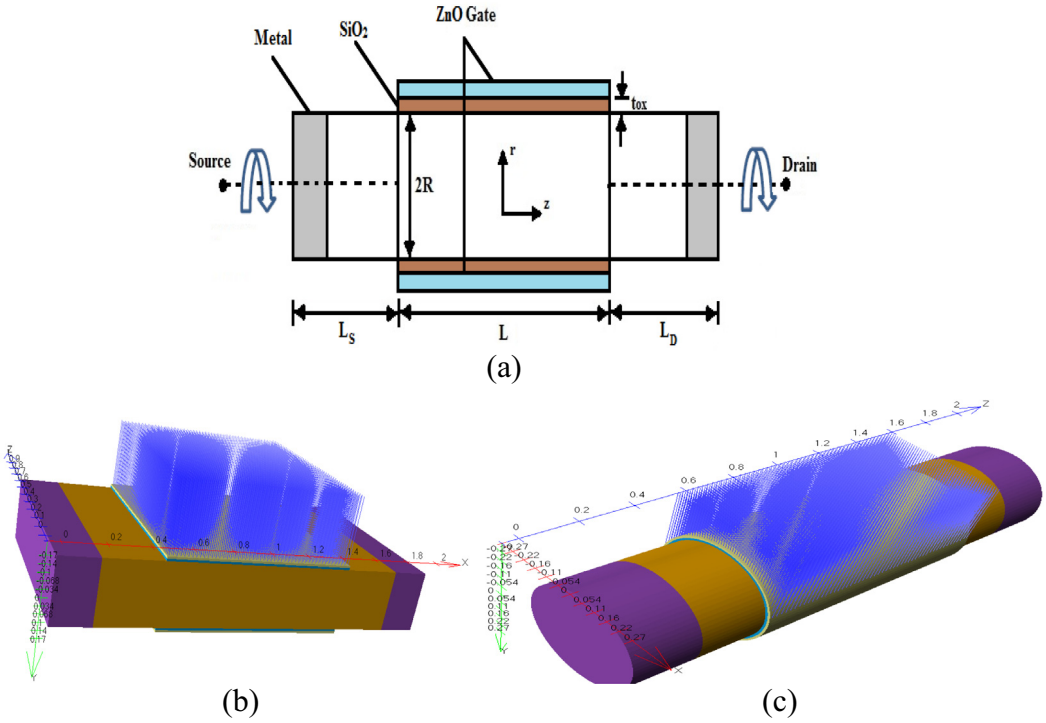


**Fig. 1.** (a) 2D-Cross Section of CSG MOSFET (b) 3D-Simulated structure of DG MOSFET under incident radiation (c) 3D-Simulated structure of CSG MOSFET under incident radiation.

**Table 2**
Real and Imaginary refractive index values for ZnO, $SiO_2$, and Si and corresponding reflection coefficients for three interfaces at different wavelengths of incident radiation [21].

| λ (nm) | Zinc Oxide (ZnO) | | | Silicon dioxide ($SiO_2$) | | | Silicon (Si) | | | |
|---|---|---|---|---|---|---|---|---|---|---|
| | $n_1$ | $k$ | $R_1$ | $n_2$ | $k$ | $R_2$ | $n_3$ | $k$ | $R_3$ | $\alpha\ (cm^{-1}) \times 10^6$ |
| 250 | 1.92 | 0.383 | 0.115 | 1.600 | 0.008 | 0 | 1.58 | 3.63 | 0.56 | 1.827 |
| 300 | 1.99 | 0.404 | 0.126 | 1.578 | 0.013 | 0 | 5.00 | 4.168 | 0.48 | 1.746 |
| 350 | 2.14 | 0.457 | 0.150 | 1.565 | 0.024 | 0 | 5.43 | 2.989 | 0.41 | 1.073 |
| 400 | 2.27 | $4 \times 10^{-3}$ | 0.151 | 1.557 | 0.035 | 0 | 5.57 | 0.387 | 0.31 | 0.121 |
| 450 | 2.11 | $4 \times 10^{-18}$ | 0.127 | 1.552 | 0.023 | 0 | 4.67 | 0.139 | 0.25 | 0.03886 |
| 500 | 2.05 | 0 | 0.119 | 1.548 | 0.019 | 0 | 4.29 | 0.069 | 0.22 | 0.01746 |
| 550 | 2.02 | 0 | 0.114 | 1.545 | 0.018 | 0 | 4.08 | 0.043 | 0.20 | 0.00985 |

three interfaces. It also shows the values of absorption coefficient (α) for Silicon at different wavelengths. The amount of incident light being absorbed by the Si channel underneath which results in the generation of electron-hole pairs (EHP) depends mainly on the absorption coefficient of Si denoted by absorption coefficient (α). The parameter α for Si has different values for different wavelengths (λ) of incident radiation and generally decreases with higher wavelengths [22,23].

Rate of generation of EHP depends upon the absorption of incident radiation by the Si channel underneath. As mentioned above the generation rate depends on the absorption coefficient of the photosensitive material which is Si in our device. The rate of generation of EHP is given by the formula [24].

$$G_r = \alpha \emptyset_d \tag{2}$$

where $\emptyset_d$ is the incident spectral photon flux density and is given by [24].

$$\emptyset_d = I_o \frac{h}{c\lambda}(1-R_1)(1-R_2)(1-R_3) \tag{3}$$

where $I_o$ is the intensity of incident radiation, $c$ is the speed of light, and $h$ is the Planck's constant.

## 3. Simulation results and discussion

Fig. 2 shows the $I_d$-$V_{gs}$ characteristics under dark as well as under incident radiation of the DG MOSFET compared with the already proposed device reported in [24] and also in accordance with previous work [25–27]. $I_d$-$V_{gs}$ characteristics of the simulated DG MOSFET as compared to the reported device have almost same variation and hence this device is used further for the sake of comparison with CSG MOSFET.

Fig. 3 shows the comparison of $I_d$-$V_{gs}$ characteristics of simulated DG MOSFET with CSG MOSFET under dark as well as under incident radiation. It can be inferred from the figure that as compared to DG MOSFET, CSG MOSFET has lower dark current and higher illumination current because of effective electrostatic coupling between gate and the channel as channel completely surrounds the silicon pillar. Fig. 4 is a result showing the variation in $I_d$-$V_{gs}$ characteristics of CSG MOSFET under different light intensities ($I_o$). As light intensity increases conductance of the channel increases which results in higher current available under incident radiation and this variation of illumination current with respect to the intensity of light is more pronounced in subthreshold region as compared to linear or saturation region and hence the proposed device works better as a UV–visible Photosensor in subthreshold region.

Fig. 5 showing the dependency of $I_d$-$V_{gs}$ characteristics on the wavelength of incident radiation. Higher the wavelength higher will be the illumination current and for channel radius R = 0.25 μm at λ = 450 nm the $I_{on}/I_{off}$ ratio is maximum. Hence the proposed device can be used in this region of spectrum as a highly efficient low power photosensor.

Responsivity and Quantum Efficiency are very important parameters of a photosensor. These parameters can be evaluated using the formula [28].

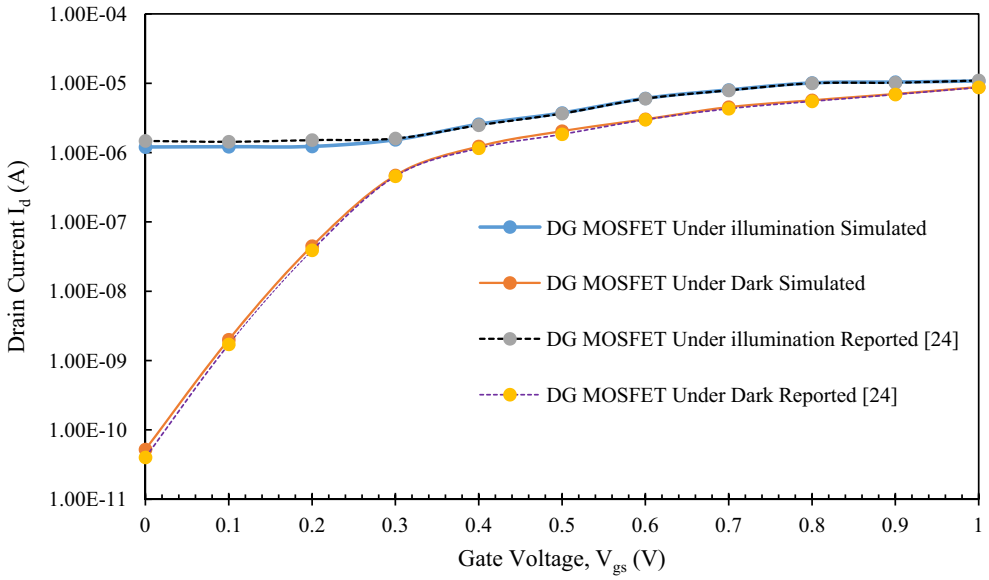


**Fig. 2.** $I_d$-$V_{gs}$ characteristics of DG MOSFET under dark and under incident radiation for simulated device and reported device. $I_0 = 10\ W/cm^2$, $V_{ds} = 0.05$ V, λ = 250 nm, $t_{si} = 0.3$ μm.

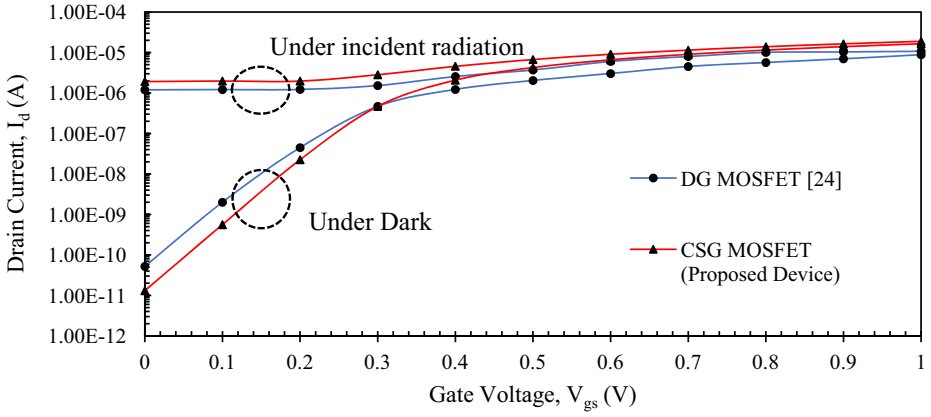


**Fig. 3.** Comparison of $I_d$-$V_{gs}$ characteristics of DG MOSFET and CSG MOSFET under dark and under incident radiation $I_0$ = 10 W/cm$^2$, $V_{ds}$ = 0.05 V, λ = 250 nm, R = 0.25 μm.

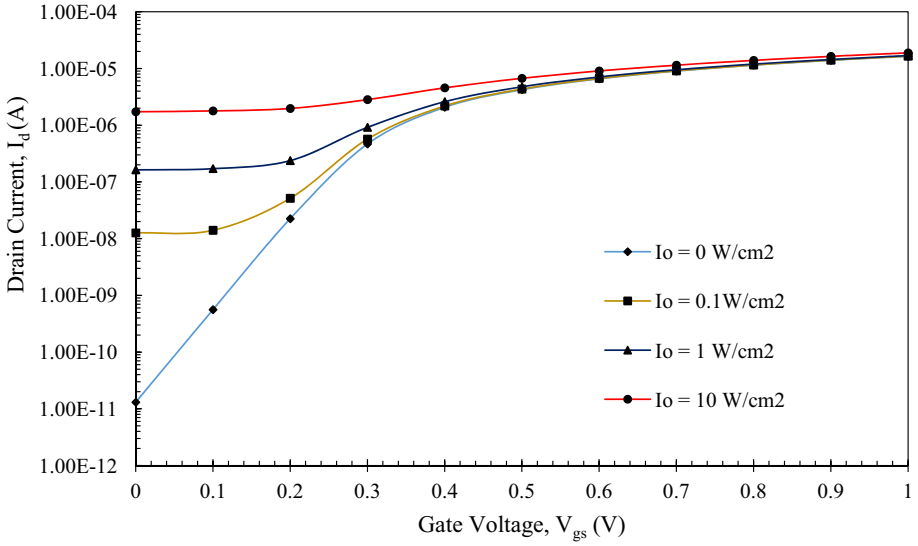


**Fig. 4.** $I_d$-$V_{gs}$ characteristics of CSG MOSFET under different intensities of incident radiation $V_{ds}$ = 0.05 V, λ = 250 nm, R = 0.25 μm.

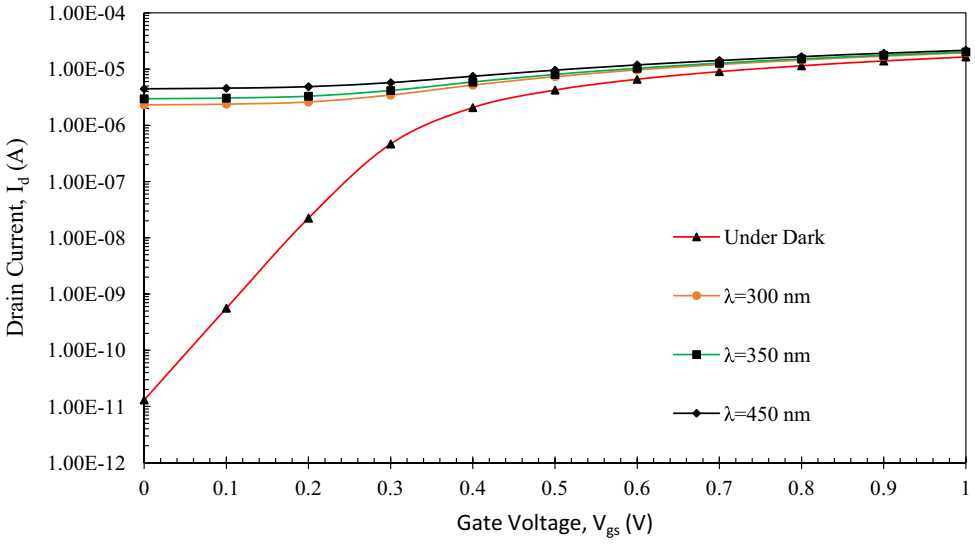


**Fig. 5.** $I_d$-$V_{gs}$ characteristics of CSG MOSFET under different wavelength of incident radiation. $V_{ds}$ = 0.05 V, $I_0$ = 10 W/cm$^2$, R = 0.25 μm.

$$Responsivity\ (R_e) = \frac{Available\ Photocurrent,\ I_{ap}\ (A)}{Incident\ Optical\ Power,\ P_o\ (W)} \quad (4)$$

$$Quantum\ Efficiency\ (Q_e) = R_e \times \frac{hc}{q\lambda} \quad (5)$$

The result in Fig. 6(a) is showing the dependency of available photocurrent on the wavelength of incident radiation for different channel radius. Clearly higher the channel radius more will be the area on which light is absorbed and hence more will be the available photocurrent. At higher wavelengths the available photocurrent decreases because of two factors firstly the energy required to detach an electron from a Si atom in the channel is not sufficient at higher wavelength. Secondly, there are decreases in the absorption coefficient as given in Table 2 at higher wavelengths. Further it can be seen that maximum absorption of light takes place over a range of λ = 250 nm to λ = 600 nm for silicon based CSG MOSFET using ZnO as transparent gate material.

Fig. 6(b) representing the dependency of responsivity of the proposed photosensor for different wavelengths of the incident radiation and varying channel radius. Observing carefully the maximum responsivity is at λ = 0.4 μm for R = 0.15 μm and λ = 0.45 μm for R = 0.25 μm. The reason for this behavior is based on the fact that when the channel radius is small effective photoabsorption can take place for the lower wavelengths of incident radiation but with the increase in channel radius higher

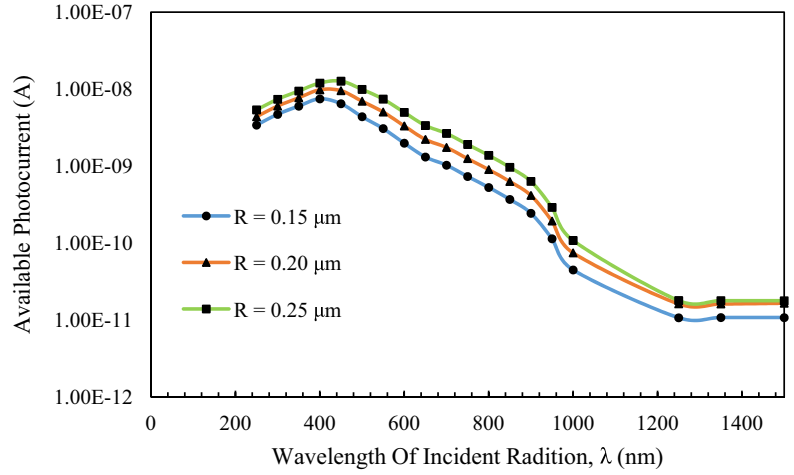


**(a)**

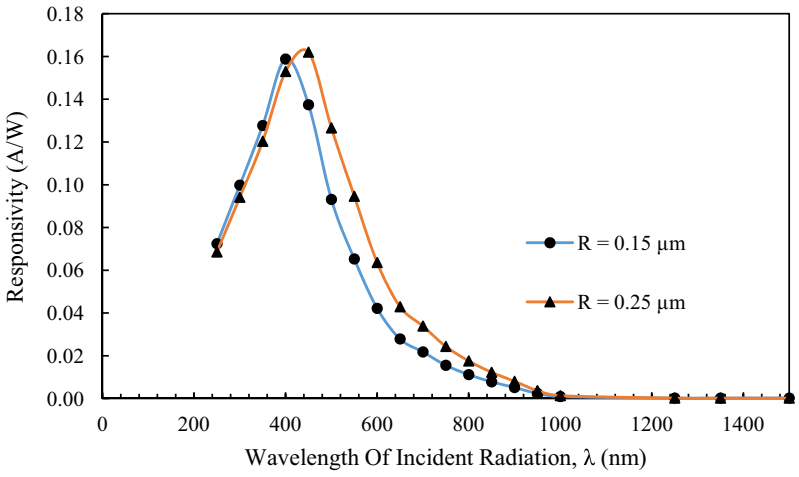


**(b)**

**Fig. 6.** (a) Available Photocurrent vs Wavelength for different Channel Radius. (b) Responsivity vs Wavelength for different Channel Radius. $I_0$ = 10 W/cm$^2$, $V_{gs}$ = 0.0 V, $V_{ds}$ = 0.05 V.

**Table 3**
Comparison of $V_{th}$, and $I_{on}/I_{off}$ ratio for DG MOSFET and CSG MOSFET for different values of the incident radiation ($I_o$) λ = 250 nm, R = 0.25 μm, $t_{si}$ = 0.3 μm, L = 1 μm, W = 1 μm.

| $I_o$ W/cm$^2$ | DG MOSFET ($V_{th}$) | CSG MOSFET ($V_{th}$) | DG MOSFET ($I_{on}/I_{off}$) | CSG MOSFET ($I_{on}/I_{off}$) |
|---|---|---|---|---|
| 0 | 0.35 | 0.310 | $1.75 \times 10^5$ | $12.6 \times 10^5$ |
| 0.1 | 0.34 | 0.302 | $0.925 \times 10^3$ | $1.30 \times 10^3$ |
| 1 | 0.30 | 0.272 | $0.716 \times 10^2$ | $1.03 \times 10^2$ |
| 10 | 0.19 | 0.212 | 7.19 | 10.9 |

wavelengths can penetrate deep inside the channel resulting in effective photo absorption [29]. Maximum responsivity of the photodetector is further affected by the bias conditions, the recombination process and by optical effects such as reflection and interference [30–32].

Table 3 shows the performance comparison of DG MOSFET with CSG MOSFET in terms of change in threshold voltage ($V_{th}$) and $I_{on}/I_{off}$ ratio with the intensity of incident radiation at $\lambda = 250$ nm. CSG MOSFET has lower threshold voltage and higher $I_{on}/I_{off}$ ratio due to effective control of gate over channel and hence lower

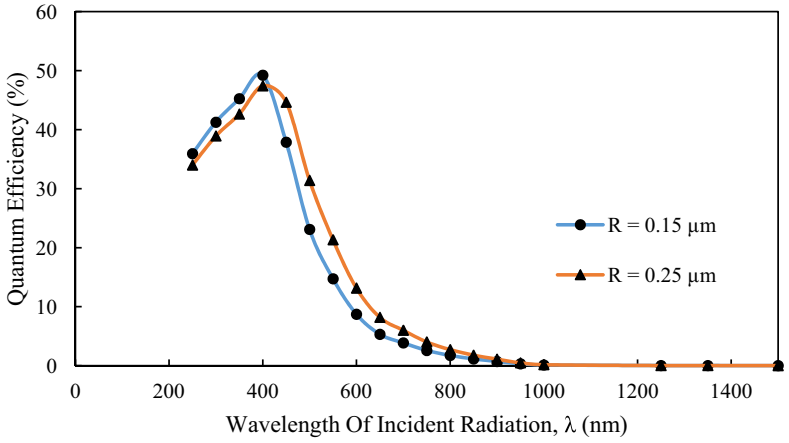


**Fig. 7.** Quantum Efficiency vs Wavelength for different Channel Radius. $I_0 = 10$ W/cm$^2$, $V_{gs} = 0.0$ V, $V_{ds} = 0.05$ V.

**Table 4**
Variation of $V_{th}$, $I_{on}$,$I_{off}$ and $I_{on}/I_{off}$ ratio for different values of the incident radiation ($I_o$). (a) R = 0.15 μm (b) R = 0.20 μm (c) R = 0.25 μm.

| $I_o$ W/cm$^2$ | $V_{th}$ (V) | $I_{on}$ (μA) | $I_{off}$ (nA) | $I_{on}/I_{off}$ |
|---|---|---|---|---|
| (*a*) | | | | |
| 0 | 0.310 | 9.94 | 0.019 | $5.20 \times 10^5$ |
| 0.1 | 0.308 | 9.96 | 7.33 | $1.35 \times 10^3$ |
| 1.0 | 0.298 | 10.1 | 88.0 | $1.14 \times 10^2$ |
| 10 | 0.242 | 11.0 | 852 | 12.91 |
| $I_o$ W/cm$^2$ | $V_{th}$ (V) | $I_{on}$ (μA) | $I_{off}$ (nA) | $I_{on}/I_{off}$ |
| (*b*) | | | | |
| 0 | 0.310 | 13.3 | 0.015 | $8.52 \times 10^5$ |
| 0.1 | 0.306 | 13.4 | 9.94 | $1.34 \times 10^3$ |
| 1.0 | 0.297 | 13.6 | 125 | $1.08 \times 10^2$ |
| 10 | 0.221 | 14.9 | 1260 | 11.8 |
| $I_o$ W/μm$^2$ | $V_{th}$ (V) | $I_{on}$ (μA) | $I_{off}$ (nA) | $I_{on}/I_{off}$ |
| (*c*) | | | | |
| 0 | 0.310 | 16.4 | 0.013 | $12.6 \times 10^5$ |
| 0.1 | 0.302 | 16.5 | 12.6 | $1.30 \times 10^3$ |
| 1.0 | 0.272 | 16.9 | 164 | $1.03 \times 10^2$ |
| 10 | 0.212 | 18.9 | 1730 | 10.9 |

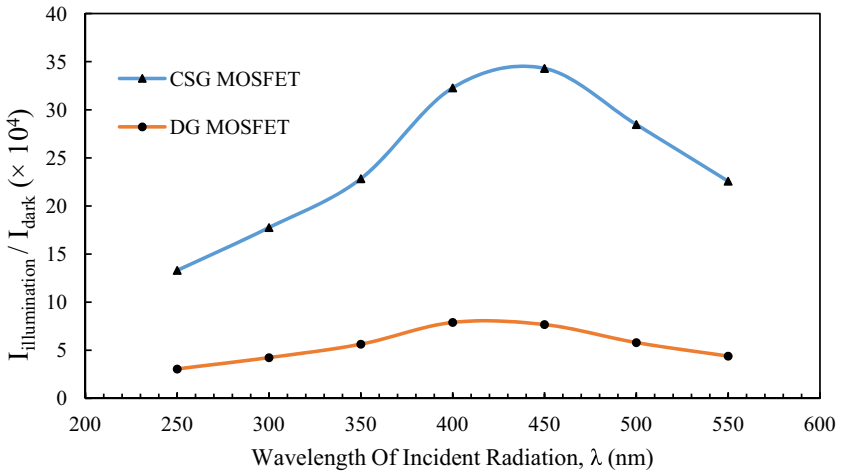


**Fig. 8.** Sensitivity vs Wavelength. $I_0 = 10$ W/cm$^2$, $V_{gs} = 0.0$ V, $V_{ds} = 0.05$ V,R = 0.25 μm.

threshold voltage and higher $I_{on}/I_{off}$ ratio in subthreshold region can be utilized to use it as a low power photosensor.

Fig. 7 is a plot of curves showing the percentage Quantum Efficiency for different wavelengths of incident radiation. Observing carefully Quantum Efficiency first increases with increase in wavelengths and then decreases after attaining a maximum value at $\lambda = 400$ nm for R = 0.15 μm and $\lambda = 450$ nm for R = 0.25 μm. Hence the proposed device can be utilized as a highly efficient photosensor in this region of spectrum. Table 4 shows the change in threshold voltage ($V_{th}$), $I_{on}$, $I_{off}$, and $I_{on}/I_{off}$ ratio with the intensity of incident radiation and radius at $\lambda = 250$ nm. Illumination causes a higher off state leakage current, a reduced subthreshold slope and a lower value for the threshold voltage. Lower threshold voltage and higher $I_{on}/I_{off}$ ratio in subthreshold region further added to its use as low power photosensing applications.

Sensitivity of the photodetector is defined as the ratio of the current obtained under illumination to that of current obtained under dark condition ($I_{illumination}/I_{dark}$). Fig. 8 is a plot showing the sensitivity variation with respect to the variation in the incident wavelength. On being exposed to light as compared to DG MOSFET, CSG MOSFET shows higher sensitivity because of higher illumination current and lower dark current. At lower side of the spectrum sensitivity is small and it peaks at $\lambda = 450$ nm for R = 0.25 μm and further decreases at the farther side of the spectrum. Hence the proposed device can be effectively used as a highly sensitive low power photosensor in visible range and can be further implemented through other FET devices like CNT [33] and Impact ionization MOS [34].

## 4. Conclusion

CSG MOSFET with ZnO as a gate material and $SiO_2$ as a gate dielectric is highly sensitive in the desired region of spectrum. The sensitivity of CSG MOSFET is 4.5 times as compared to DG MOSFET and peak sensitivity is observed at $\lambda = 450$ nm for channel radius R = 0.25 μm and hence can be effectively used as a highly sensitive photosensor in this region of spectrum. The proposed device also shows higher illumination current in the subthreshold region under incident radiation, lower threshold voltage and higher $I_{on}/I_{off}$ ratio so for low power operation the device can be biased in subthreshold region for optimum performance. ZnO as a gate material act as an optical filter which allows only visible region wavelengths to pass through it and blocks other wavelengths from reaching the Si channel underneath and hence maximum photoabsorption takes place for visible wavelength which make this device to work efficiently for Photodetection in the visible region.

## References


[1] X. Gong, M.H. Tong, Y.J. Xia, W.Z. Cai, J.S. Moon, Y. Cao, G. Yu, C.L. Shieh, B. Nilsson, A.J. Heeger, High-detectivity polymer photodetectors with spectral response from 300 nm to 1450 nm, Science 325 (2009) 1665–1667.

[2] C.W. Liu, C.H. Lin, Metal-insulator-semiconductor photodetectors, Sensors 10 (2010) 8797–8826.

[3] H.W. Lin, S.Y. Ku, H.C. Su, C.W. Huang, Y.T. Lin, K.T. Wong, C.C. Wu, Highly efficient visible-blind organic ultraviolet photodetectors, Adv. Mater. 17 (2005) 2489–2493.

[4] G. Sarasqueta, K.R. Choudhury, J. Subbiah, F. So, Organic and inorganic blocking layers for solution-processed colloidal PbSe nanocrystal infrared photodetectors, Adv. Funct. Mater. 21 (2011) 167–171.

[5] G. Konstantatos, I. Howard, A. Fischer, S. Hoogland, J. Clifford, E. Klem, L. Levina, E.H. Sargent, Ultrasensitive solution-cast quantum dot photodetectors, Nature 442 (2006) 180–183.

[6] M. Ettenberg, A little night vision, Adv. Imaging 20 (2005) 29–32.

[7] Fuxi Gan, Lisong Hou, Guangbin Wang, Huiyong Liu, Jing Li, Optical and recording properties of short wavelength optical storage materials, Mater. Sci. Eng. B 76 (1) (2000) 63–68.

[8] H. Cho, P. Kapur, K.C. Saraswat, Power comparison between highspeed electrical and optical interconnects for interchip communication, J. Lightwave Technol. 22 (2004) 2021–2033.

[9] Hal L. Levitt, Y. Tse Anthony, Signal processing apparatus, U.S. Patent 5,682,238, issued October 28, 1997.

[10] Yaocheng Liu, Kavitha Gopalakrishnan, Peter B. Griffin, Kai Ma, Michael D. Deal, James D. Plummer, MOSFETs and high-speed photodetectors on Ge-on-insulator substrates fabricated using rapid melt growth, in: Electron Devices Meeting, 2004, IEDM Technical Digest, IEEE International, IEEE, 2004, pp. 1001–1004.

[11] T. Ando, C.K. Fong, Photoresponses in $In_2O_3$ transparent gate MOS capacitors, IEEE Trans. Electron Devices 29 (8) (1982) 1161–1167.

[12] N.S. Roy, B.B. Pal, R.U. Khan, Analysis of GaAs OPFET with improved optical absorption under back illumination, IEEE Trans. Electron Devices 46 (1999) 2351–2353.

[13] S.E. Holland, N.W. Wang, W.W. Moses, Development of low noise, back-side illuminated silicon photodiode arrays, IEEE Trans. Nucl. Sci. 44 (1997) 443–447.

[14] Pei-Nan Ni, Chong-Xin Shan, Shuang-Peng Wang, Bing-Hui Li, Zhen-Zhong Zhang, Dong-Xu Zhao, Lei Liu, De-Zhen Shen, Enhanced responsivity of highly spectrum-selective ultraviolet photodetectors, J. Phys. Chem. C 116 (1) (2011) 1350–1353.

[15] H. Zimmermann, Integrated high speed, high sensitivity photodiodes and optoelectronic integrated circuits, Sens. Mater. 13 (4) (2001) 189–206.

[16] A. Stoykov, R. Scheuermann, Silicon Avalanche Photodiodes, Laboratory for Muon Spin Spectroscopy, Paul Scherrer Institut, 2004.

[17] R.A. Ismail, W.K. Hamoudi, Characteristics of novel silicon pin photodiode made by rapid thermal diffusion technique, J. Electron Devices 14 (2012) 1104–1107.

[18] A. Pal, A. Sarkar, Analytical study of dual material surrounding gate MOSFET to suppress short-channel effects (SCEs), Eng. Sci. Technol. Int. J. 17 (4) (2014) 205–212.

[19] ATLAS User's Manual 3-D Device Simulator, SILVACO International, Version 5.14.0.R, 2010.

[20] S.M. Sze, Physics of Semiconductor Devices, second ed., John Wiley and Sons, 1981. p. 804.

[21] SOPRA infobase, <http://refractiveindex.info>.

[22] P. Chakrabarti, N.L. Shrestha, S. Srivastava, V. Khemka, An improved model of ion-implanted GaAs OPFET, IEEE Trans. Electron Devices 39 (9) (1992).

[23] M.L. Simpson, M.N. Ericson, G.E. Jellison Jr., W.B. Dress, A.L. Wintenberg, M. Bobrek, Application specific spectral response with CMOS compatibility photodiodes, IEEE Trans. Electron Devices 46 (5) (1999) 905–913.

[24] R. Gautam, M. Saxena, R.S. Gupta, M. Gupta, Analytical model of double gate MOSFET for high sensitivity low power photosensor, J. Semicond. Technol. Sci. 13 (5) (2013).

[25] S.K. Sharma, B. Raj, M. Khosla, A Gaussian approach for analytical subthreshold current model of cylindrical nanowire FET with quantum mechanical effects, Microelectron. J. 53 (2016) 65–72.

[26] S.K. Sharma, B. Raj, Khosla, Subthreshold performance of $In_{1-x}Ga_xAs$ based dual metal gate stack cylindrical/surrounding gate nanowire MOSFET for low power analog applications, J. Nanoelectron. Optoelectron. 11 (2016) 1–6.

[27] S.K. Sharma, B. Raj, Khosla, Comparative analysis of MOSFET, CNTFET and NWFET for energy efficient VLSI circuit design, J. VLSI Des. Tools Technol. 6 (2) (2016) 1–6.

[28] O. Bazkir, Quantum efficiency determination of unbiased silicon photodiode and photodiode based trap detectors, Rev. Adv. Mater. Sci. 21 (2009) 90–98.

[29] H.-D. Um, S.A. Moiz, K.T. Park, J.Y. Jung, S.W. Jee, C.H. Ahn, D.C. Kim, H.K. Cho, D.W. Kim, J.H. Lee, Highly selective spectral response with enhanced responsivity of n-ZnO/p-Si radial heterojunction nanowire photodiodes, Appl. Phys. Lett. 98 (2011). 033102-3.

[30] E. Lee, D. Moon, J.H. Yang, K.S. Lim, Y.K. Choi, Transparent zinc oxide gate metal-oxide-semiconductor field effect transistor for high responsivity photodetector, IEEE Trans. Device Lett. 30 (5) (1999) 2351–2353.

[31] K. Das et al., Single Si nanowire (diameter $\leqslant$100 nm) based polarization sensitive near-infrared photodetector with ultra-high responsivity, Nanoscale 6 (19) (2014) 11232–11239.

[32] Kyungwhan Yang, Kiyeol Kwak, Sangsig Kim, Influence of the intrinsic length on $p^+$-i-$n^+$ Si nanowire avalanche photodetectors on flexible plastic substrates, Phys. Status Solidi C 11 (2) (2014) 217–221.

[33] M.H. Moaiyeri, M. Nasiri, N. Khastoo, An efficient ternary serial adder based on carbon nanotube FETs, Eng. Sci. Technol. Int. J. 19 (1) (2016) 271–278.

[34] S. Singh, P.N. Kondekar, Analytical modeling of Schottky tunneling source impact ionization MOSFET with reduced breakdown voltage, Eng. Sci. Technol. Int. J. 19 (1) (2016) 421–428.